Robotica: (2021) volume 39, pp. 618–632. © The Author(s), 2020. Published by Cambridge University Press.
doi:10.1017/S0263574720000624

Dynamics Modeling of Human–Machine Control Interface for Underwater Teleoperation

Giovanni Gerardo Muscolo†*, Simone Marcheschi‡, Marco Fontana¶ and Massimo Bergamasco‡

†*DIMEAS-Department of Mechanical and Aerospace Engineering, Politecnico di Torino, Corso Duca degli Abruzzi, 24, 10129, Torino, Italy. E-mail: giovanni.muscolo@polito.it*
‡*TeCIP Institute, Sant'Anna School of Advanced Studies, Via Alamanni 13B, San Giuliano Terme, Pisa, 56010, Italy. E-mails: {simone.marcheschi; massimo.bergamasco}@santannapisa.it*
¶*Dipartimento di Ingegneria Industriale, University of Trento, Via Sommarive, 9, 38123 Povo, Trento, Italy. E-mail: marco.fontana-2@unitn.it*

(Accepted June 20, 2020. First published online: July 22, 2020)

SUMMARY
This paper presents an experimental study on new paradigms of haptic-based teleoperated navigation of underwater vehicles. Specifically, the work is focused on investigating the possibility of enhancing the user interaction by introducing haptic cues at the level of the user wrist providing a force feedback that reflects dynamic forces on the remotely operated underwater vehicle. Different typologies of haptic controllers are conceived and integrated with a real-time simulated model of an underwater robotic vehicle. An experimental test is designed to evaluate the usability of the system and to provide information on the global performance during the execution of simple tasks. Experiments are conducted with 7 candidates testing 12 different controllers. Among these, the most effective strategies have been identified and selected on the basis of minimization of errors on the vehicle trajectory and of the quality of the user's interaction in terms of perceived comfort during operation. Overall, the results obtained with this study underline that haptic navigation control can have a positive influence on the performance of remotely controlled underwater vehicles.

KEYWORDS: Underwater teleoperation; Haptic interface; Underwater vehicle; Human–machine control interface; Robotics.

1. Introduction

The worldwide demand of underwater operations is constantly increasing in the last decades.[1–5] Oil and gas, marine renewable energy, telecommunications, energy, military, scientific studies, and construction of ocean observatories are only few examples of applications in which underwater operations are needed. The types of task to be performed in deep waters can be of different nature, such as visual inspection,[6] material, or object sampling,[7–9] manipulation of instrumentations and controls,[3,10,11] and drilling.[12] Only few of these tasks can be performed under direct control of *in situ* operators since the working depth is often not accessible to humans.[13] For these reasons remotely operated vehicles (ROV) or autonomous underwater vehicles (AUV) are often employed, with the former one being used in most of the cases where direct interaction with the environment is required.[14–17] The remote control of ROV includes the control of navigation, that is, the control ofthe position and orientation of the vehicle, and the control of onboard tools, that is, the control of

* Corresponding author. E-mail: giovanni.muscolo@polito.it

https://doi.org/10.1017/S0263574720000624 Published online by Cambridge University Press

on-board grippers, manipulators or other specialized tools. Such control requires a human computer interface and is conventionally implemented through simple devices such as joysticks, gamepads, or buttons.[18] It is recognized that this mode of interaction can be effective in many simple scenarios but due to the lack of intuitiveness can be quite limited in more complex tasks.

Several research activities have been conducted with the aim of improving the quality and the performance of telecontrol of these vehicles. Immersive visual systems,[19] motion capture devices,[6] and haptic interfaces have been introduced to enhance the usability.[20] Specifically, haptics have been largely investigated in combination with on-board robotic manipulator[20–22] to provide a force feedback that is proportional to the forces applied on the remote environments. On the contrary, the possibility of exploiting haptic feedback to support navigation tasks is less explored.[23] A previous research[24] showed the possibility of introducing artificial force field on the basis of obstacles in the proximity of the mobile vehicle in order to prevent dangerous contacts. Additionally, the idea of using haptic device to provide information about the working environment back to the operator during navigation is investigated.[25] In particular, the drag force generated by the fluid interaction has been chosen as the feedback objective for the haptic control. However, the investigation is limited to the only surge motion of the ROV. Thus, the multidimensionality of the ROV trajectories is not replicated.

In this paper, we introduce a novel paradigm of navigation control of ROV in which, beside visual feedback, haptic cues are delivered on the wrist of the user to provide feeling of the dynamics forces experienced by the remote vehicle. The proposed underwater haptic control system is integrated in a real-time modeling environment to drive a hybrid remotely operated vehicle (HROV)[13] integrating the GRAB haptic interface.[26] The proposed haptic control system has been tested on subjects with the final aim to evaluate the user experience and performance. Tests on the developed haptic control system have been performed driving a simplified model of the ODIN underwater vehicle,[27–31] designed at Autonomous Systems Laboratory of the University of Hawaii, which is a benchmark and many details on its model are available in literature.[27–31] Seven voluntary candidates tested the haptic system driving the vehicle. Tests performed have helped to define a standard haptic control system used for underwater vehicles.

The paper is structured as follows: Section 2 shows the dynamics modeling for underwater vehicles; Section 3 presents the control architecture for underwater teleoperation; Section 4 shows the performed experimentations, results, and discussion. The paper ends with conclusion and future works.

2. Dynamics Modeling for Underwater Vehicles

2.1. Coordinate system

In order to describe the motion of an underwater robotic vehicle (URV), we assume the notation of The Society of Naval Architects and Marine Engineers (SNAME).[32–38] Specifically, as represented in Fig. 1, we assume a body-fixed coordinate system with the origin located at the vehicle's center of buoyancy, which is assumed to be constant with respect to the vehicle since we are not considering possible changes in shapes or volumes. The general motion of the vehicle has six degrees of freedom and can be described by the following vectors: $\eta_1 = [x\ y\ z]^T$, $\eta_2 = [\phi\ \theta\ \psi]^T$; $\nu_1 = [u\ v\ w]^T$, $\nu_2 = [p\ q\ r]^T$, $\tau_1 = [X\ Y\ Z]^T$; and $\tau_2 = [K\ M\ N]^T$, where $\eta = [\eta_1\ \eta_2]^T$ describes the position and orientation of the vehicle with respect to the inertial or earth fixed reference frame, $\nu = [\nu_1 \nu_2]^T$ the translational and rotational velocities of the vehicle with respect to the body-fixed reference frame, and $\tau_\nu = [\tau_1\ \tau_2]^T$ the total forces and moments acting on the vehicle with respect to the body-fixed reference frame. The angles ϕ, θ, ψ (azimuth, elevation, and spin) are related through Euler transformations to the body yaw, pitch, and roll motions.

A relation between the velocity of the vehicle and the derivatives of the two reference frames is:

$$\nu = \mathrm{J_e}(\mathrm{R_B^I})\dot{\boldsymbol{\eta}}, \tag{1}$$

$$\mathrm{J}_e(\mathrm{R}_B^I) = \begin{bmatrix} \mathrm{R}_B^I & \mathrm{O}_{3\times3} \\ \mathrm{O}_{3\times3} & \mathrm{J}_{k,o} \end{bmatrix}, \tag{2}$$

https://doi.org/10.1017/S0263574720000624 Published online by Cambridge University Press

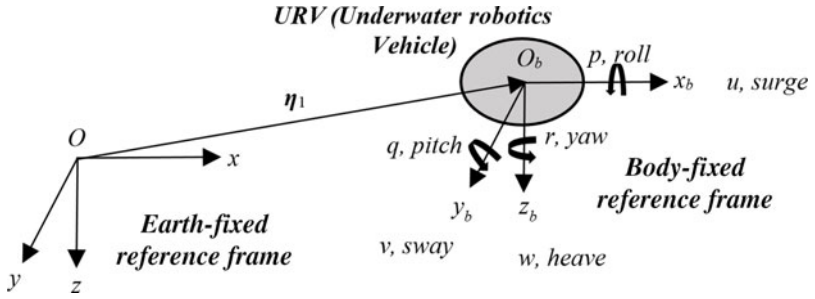


Fig. 1. Earth-fixed and body-fixed reference frames in underwater vehicle definition.

where R_B^I is the rotation matrix expressing the transformation from the inertial frame to the body-fixed frame. $\mathrm{O}_{3\times3}$ is the null matrix.

$$\mathrm{J}_{k,o}(\eta_2) = \begin{bmatrix} 1 & 0 & -s\theta \\ 0 & c\phi & c\theta s\phi \\ 0 & -s\phi & c\theta c\phi \end{bmatrix}, \tag{3}$$

where $\sin\theta = s\theta$, $\cos\theta = c\theta$, $\sin\phi = s\phi$, $\cos\phi = c\phi$, $\sin\psi = s\psi$, and $\cos\psi = c\psi$.

2.2. Dynamic model of underwater vehicles with thrusters

The equations of motion can be written for the notation that is assumed in the previous subsection as:[32]

$$\mathrm{M}_v^*\ddot{\eta} + \mathrm{C}_v^*\dot{\eta} + \mathrm{D}_{RB}^*\dot{\eta} + \mathbf{g}_{RB}^* = \tau_v^* - \tau_{v,c}^*, \tag{4}$$

where

$$\mathrm{M}_v^* = \mathrm{M}_v^*\left(\mathrm{R}_B^I\right) = \mathrm{J}_e^{-T}\left(\mathrm{R}_B^I\right)\left(\mathrm{M}_{RB} + \mathrm{M}_A\right)\mathrm{J}_e^{-1}\left(\mathrm{R}_B^I\right), \tag{5}$$

$$\mathrm{C}_v^* = \mathrm{C}_v^*\left(\mathrm{R}_B^I, \dot{\eta}\right) = \mathrm{J}_e^{-T}\left(\mathrm{R}_B^I\right)\mathrm{P}\mathrm{J}_e^{-1}\left(\mathrm{R}_B^I\right), \tag{6}$$

and

$$\mathrm{P} = \left(\mathrm{C}_{RB}(\mathbf{v}) + \mathrm{C}_A\right) - \left(\mathrm{M}_{RB} + \mathrm{M}_A\right)\mathrm{J}_e^{-1}\left(\mathrm{R}_B^I\right)\dot{\mathrm{J}}\left(\mathrm{R}_B^I\right), \tag{7}$$

$$\mathrm{D}_{RB}^* = \mathrm{D}_{RB}^*\left(\mathrm{R}_B^I, \dot{\eta}\right) = \mathrm{J}_e^{-T}\left(\mathrm{R}_B^I\right)\mathrm{D}_{RB}(\mathbf{v})\mathrm{J}_e^{-1}\left(\mathrm{R}_B^I\right), \tag{8}$$

$$\mathbf{g}_{RB}^* = \mathbf{g}_{RB}^*\left(\mathrm{R}_B^I\right) = \mathrm{J}_e^{-T}\left(\mathrm{R}_B^I\right)\mathbf{g}_{RB}\left(\mathrm{R}_B^I\right), \tag{9}$$

$$\tau_v^* = \mathrm{J}_e^{-T}\left(\mathrm{R}_B^I\right)\tau_v. \tag{10}$$

The matrices shown in equations represents: the mass of the vehicle (M_{RB}), the Coriolis and centripetal terms ($\mathrm{C}_{RB}(\mathbf{v})$), and the added mass terms (M_A and C_A) which represent the contribution of the fluid reaction force. $\mathrm{D}_{RB}(\mathbf{v})$ is the matrix of the damping effects (dissipative drag and lift forces on the body caused by the viscosity of the fluid). $\mathbf{g}_{RB}(\mathrm{R}_B^I)$ is the vector of the gravitational force and the buoyancy. $\tau_v = [\tau_1\ \tau_2]^T$ is the vector of total forces and moments acting on the vehicle with respect to the body-fixed reference frame. $\tau_{v,c}^*$ is the vector of the effects of specific disturbances such as waves, wind, and ocean current. Currents can be very different due to local climatic and/or geographic characteristics.[32]

In this paper, we assume that the ocean current, expressed in the inertial frame, $\mathbf{v}_C = [v_{C,x}\ v_{C,y}\ v_{C,z}\ 0\ 0\ 0]^T$ is constant and irrotational. In some papers, the effect of the current is simply modeled as a time-varying, vehicle-fixed, disturbance $\tau_{v,c}^*$. By taking into account the inertial generalized forces, the hydrodynamic effects, the gravity and buoyancy contribution, and the thruster's

https://doi.org/10.1017/S0263574720000624 Published online by Cambridge University Press

effect, it is possible to rewrite the equations of motion of a general underwater vehicle in matrix form and in terms of body-fixed coordinates:

$$(\mathrm{M}_{RB} + \mathrm{M}_A)\dot{\mathbf{v}} + (\mathrm{C}_{RB} + \mathrm{C}_A)\mathbf{v} + \mathrm{D}_{RB}\mathbf{v} + \mathbf{g}_{RB}\left(\mathrm{R}_B^I\right) = \tau, \tag{11}$$

where

$$\tau = \tau_v - \tau_{v,c}. \tag{12}$$

The matrix M_{RB} is constant, symmetric, and positive definite.

$$\mathrm{M}_{RB} = \begin{bmatrix} m\mathrm{I}_3 & -m\mathrm{S}(\mathbf{r}_c^b) \\ m\mathrm{S}(\mathbf{r}_c^b) & \mathrm{I}_{Ob} \end{bmatrix}, \tag{13}$$

$\mathbf{r}_c^b$ is the vector position from the origin of the body-fixed frame to the center of mass expressed in the body-fixed frame. S is the skew-symmetric operator. I_3 is the (3×3) identity matrix, and I_{Ob} is the inertia tensor expressed in the body-fixed frame. A unique parameterization of the matrix C_{RB} does not exist. It can be demonstrated that the matrix C_{RB} can always be parameterized such that it is skew-symmetrical; explicit expressions for C_{RB} can be found, for example, in ref. [32].

The relationship between the force/moment acting on the vehicle and the control input of the thrusters is highly nonlinear. In general, thrusters are the main cause of limit cycle in vehicle positioning and bandwidth constraint. The theory of fluid dynamics is rather complex, and it is difficult to develop a reliable model for most of the hydrodynamic effects. In literature, it is well known that kinematic and dynamic coupling between vehicle and manipulator cannot be neglected,[15,39] while most of the hydrodynamic effects have no significant influence in the range of the operative velocities.

Assuming that the vehicle is completely submerged in the water, its speed is low and it has three planes of symmetry, the following structure of matrices M_A and C_A may be considered:[27]

$$\mathrm{M}_A = -\mathrm{diag}(X_{\dot{u}}, Y_{\dot{v}}, Z_{\dot{w}}, K_{\dot{p}}, M_{\dot{q}}, N_{\dot{r}}), \tag{14}$$

where the diagonal mass coefficients represent the six components of the hydrodynamic forces and moments (X, Y, Z, K, M, N) due to the six accelerations $(\dot{u}, \dot{v}, \dot{w}, \dot{p}, \dot{q}, \dot{r})$.

$$\mathrm{C}_A = \begin{bmatrix} 0 & 0 & 0 & 0 & -Z_{\dot{w}}w & Y_{\dot{v}}v \\ 0 & 0 & 0 & Z_{\dot{w}}w & 0 & -X_{\dot{u}}u \\ 0 & 0 & 0 & -Y_{\dot{v}}v & X_{\dot{u}}u & 0 \\ 0 & -Z_{\dot{w}}w & Y_{\dot{v}}v & 0 & -N_{\dot{r}}r & M_{\dot{q}}q \\ Z_{\dot{w}}w & 0 & -X_{\dot{u}}u & N_{\dot{r}}r & 0 & -K_{\dot{p}}p \\ -Y_{\dot{v}}v & X_{\dot{u}}u & 0 & -M_{\dot{q}}q & K_{\dot{p}}p & 0 \end{bmatrix}. \tag{15}$$

The added mass coefficients can be theoretically derived by the geometry of the rigid body.[32] May be noted that, if a sphere is submerged in a fluid, a pure rotational motion of the sphere does not involve any fluid movement, that is, it is not necessary to add an inertia term due to the fluid. The viscosity of the fluid also causes the presence of dissipative drag and lift forces on the body. A common simplification is to consider only linear and quadratic damping terms and group these terms in the matrix D_{RB} such that $\mathrm{D}_{RB}(\mathbf{v}) > 0 \ \forall \ \mathbf{v} \in \Re^6$. The coefficients of this matrix are also considered to be constant. For a completely submerged body, the following further assumption can be made:[27]

$$\mathrm{D}_{RB} = -\mathrm{diag}(X_u, Y_v, Z_w, K_p, M_q, N_r) - \mathrm{diag}(A), \tag{16}$$

where

$$A = X_{u|u|}|u|, Y_{v|v|}|v|, Z_{w|w|}|w|, K_{p|p|}|p|, M_{q|q|}|q|, N_{r|r|}|r|. \tag{17}$$

https://doi.org/10.1017/S0263574720000624 Published online by Cambridge University Press

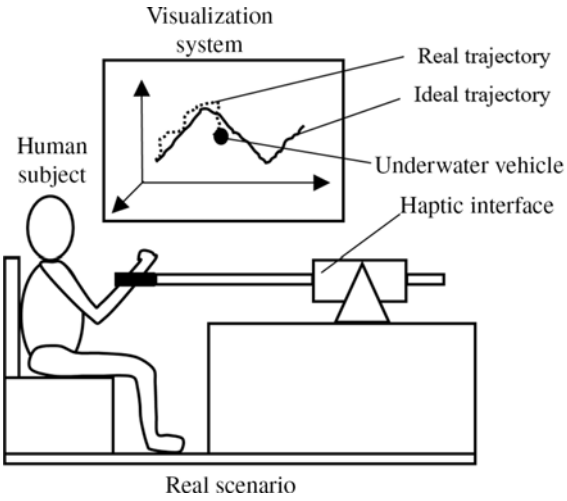


Fig. 2. Sketch of the real scenario including the human subject.

The relationship between the *force/moment* acting on the vehicle $\tau_v \in \Re^6$ and the control input of the thrusters $\mathbf{u}_v \in \Re^p$ is highly nonlinear. A common simplification is to consider a linear relationship between τ_v and $\mathbf{u}_v$:

$$\tau_v = \mathrm{B}_v \mathbf{u}_v. \tag{18}$$

On the other hand, if the vehicle is controlled by thrusters, each of which is locally fed back, the effects of the nonlinearities discussed above are very limited and a linear input–output relation between desired force/moment and the thruster's torque is experienced. This is the case, for example, of ODIN underwater vehicle,[27–31] where the experimental results show that the linear approximation is reliable. $\mathrm{B}_v \in \Re^{6xp}$ is named thruster control matrix and for the ODIN has the following expression:[27]

$$\mathrm{B}_v = \begin{bmatrix} * & * & * & * & 0 & 0 & 0 & 0 \\ * & * & * & * & 0 & 0 & 0 & 0 \\ 0 & 0 & 0 & 0 & * & * & * & * \\ 0 & 0 & 0 & 0 & * & * & * & * \\ 0 & 0 & 0 & 0 & * & * & * & * \\ * & * & * & * & 0 & 0 & 0 & 0 \end{bmatrix}, \tag{19}$$

where $*$ means a nonzero constant factor depending on the thruster collocation.

3. Modeling of Underwater Teleoperation

3.1. Haptic control underwater architecture

The interaction scenario of remote haptic guidance of an underwater vehicle is represented in Fig. 2. The human subject uses the haptic interface to control the trajectory of the underwater vehicle in marine environment. The visualization system acts as the main feedback for the control of the task. The haptic interface interacts with the human with a force which influences the motion of the human wrist on the basis of errors between actual and ideal performed trajectory.

The general control architecture (shown in Fig. 3 is composed of three blocks: H (human subject block), GRAB (haptic interface block), and UTS (underwater teleoperated system block). The GRAB block receives as input the human force ($\mathbf{F}_H$) (or position ($\mathbf{p}_H$)) with the force disturb ($\mathbf{F}_D$) and gives to the UTS block a vector position ($\mathbf{p}$) of the wrist which is scaled in the underwater vehicle domain, using the G/U (grab/underwater) control block. The desired position is the input of the remotely operated vehicle (ROV) control block and a first output is the torque for the thrusters of the URV,

https://doi.org/10.1017/S0263574720000624 Published online by Cambridge University Press

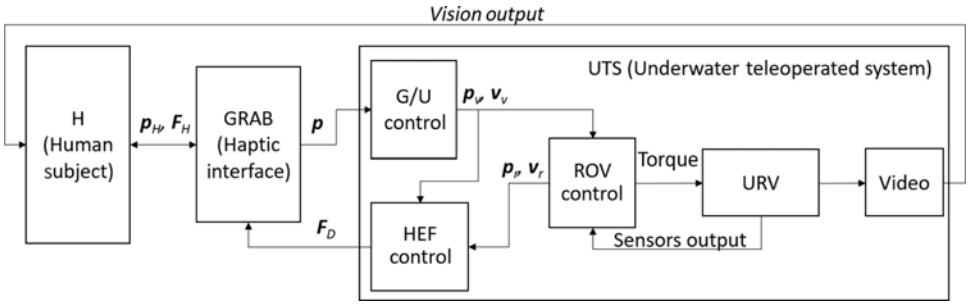


Fig. 3. General control architecture composed by human subject (H), haptic interface (GRAB), and underwater teleoperated system (UTS) blocks.

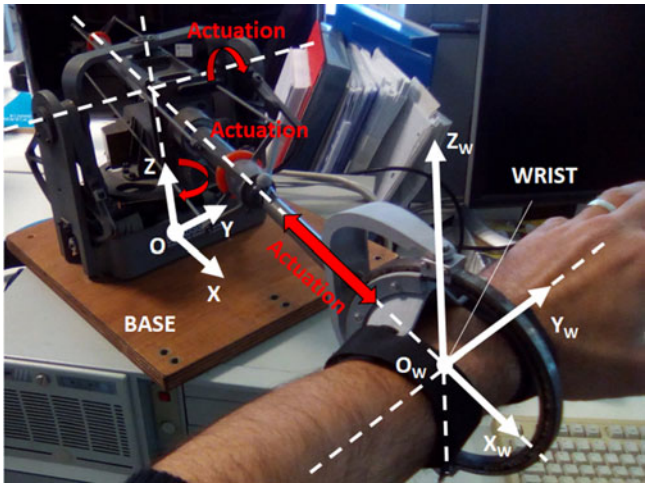


Fig. 4. GRAB haptic interface.

in order to reproduce the ideal trajectory. An error function between the two trajectories (actual and ideal) of the URV generates the force disturb ($\mathbf{F}_D$) in the human error feedback (HEF) block.

In summary, the UTS block receives as input the human wrist position ($\mathbf{p}$) and gives a vision output and a force ($\mathbf{F}_D$) that is commanded to the user wrist through the haptic interface.

3.2. GRAB: Haptic interface control system

The GRAB haptic interface presented in ref. [26] and shown in Fig. 4 has been used in this work. It is a 2R1P3R robotics arm composed by a fixed base, two actuated revolute joints, one actuated prismatic joint, and three passive revolute joints of the wrist, attached to the human wrist. Figure 5 shows the GRAB kinematic chain. The center of the robotic wrist (O_w) is coincident to the center of the human wrist.

The two reference systems shown in Figs. 4 and 5 are positioned as shown in Fig. 1, where the point O_w is coincident with the point O_b.

Figure 6 shows the control architecture of the GRAB haptic interface. The force ($\mathbf{F}$) is filtered by the system and is used to calculate the motor torque in each joint. Two control systems of position and compensation allow to obtain the vector position of the end effector (coincident with the point O_w).

3.3. UTS: Underwater teleoperated system

In this work, we employ a virtual model of the vehicle developed at the University of Hawaii and named ODIN III (Omni Directional Intelligent Navigator).[27–31] A sketch of the vehicle is shown in Fig. 7. ODIN III has a near-spherical shape with horizontal diameter of 0.63 m and vertical diameter of 0.61 m, made of anodized aluminum ($AL6061 - T6$). Table I shows the sensors used on the

https://doi.org/10.1017/S0263574720000624 Published online by Cambridge University Press

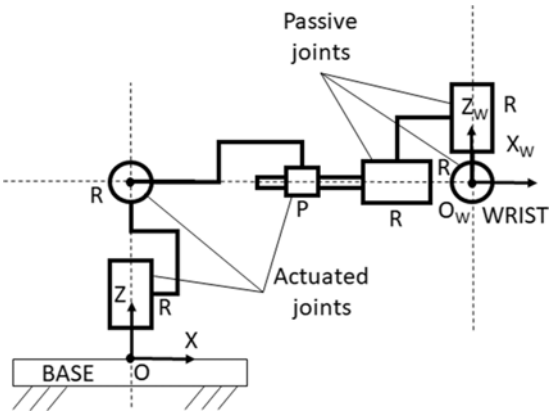


Fig. 5. Sketch of the GRAB kinematic chain: 2R1P3R.

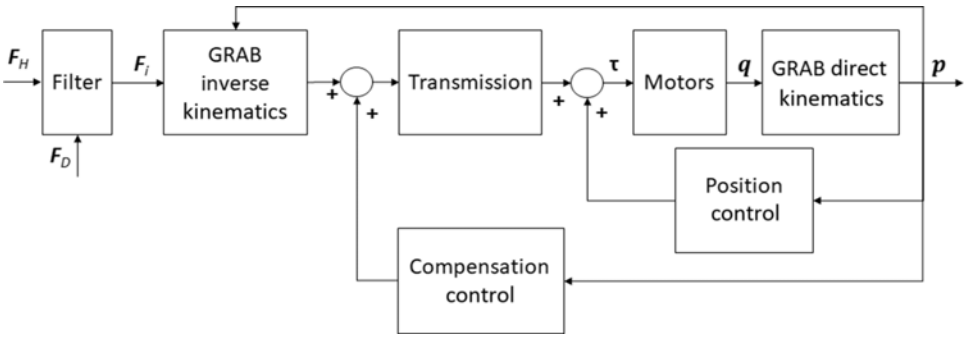


Fig. 6. GRAB (haptic interface control system) block.

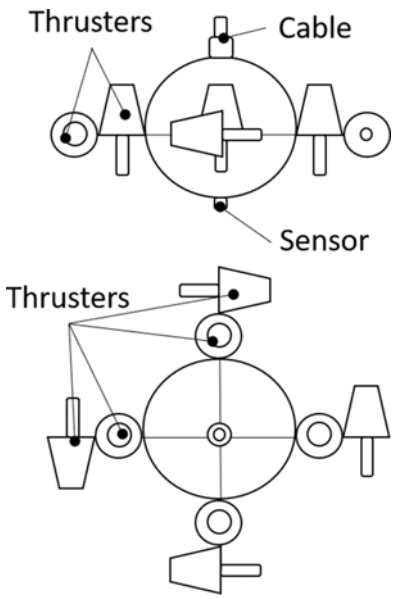


Fig. 7. Sketch of the ODIN III underwater vehicle: Side view (up); top view (down).

ODIN III.[27–31] They are used on board of the vehicle in order to give a feedback on the local position and velocity of the ODIN for the closed loop of the control system. For the numerical simulations and experiences the values shown in Tables II and III are assumed for physical variables of the vehicle.[27–31] The buoyancy B is computed considering the vehicle as spherical. The matrix B_v is

https://doi.org/10.1017/S0263574720000624 Published online by Cambridge University Press

Table I. ODIN III sensors.[27–31]

Measured variable	**Sensor**	**Rate (Hz)**
xy vehicle position	8 sonars	3
Depth	Pressure sensor	30
Roll, pitch, and yaw	IMU	30

Table II. ODIN III dimensional characteristics.[27–31]

Dimensional	**Values**
Vehicle radius	0.3 m
Vehicle weight	125 kg
$\mathbf{r}_G^B$	$[0, 0, 0.5]^T$ m
$\mathbf{r}_B^B$	$[0, 0, 0]^T$ m
$W = \text{mg}$	1226 N
$I_x = I_y = I_z$	8 Nms^2
$I_{xy} = I_{yz} = I_{xz}$	0 Nms^2

Table III. Hydrodynamic derivatives.[27–31]

Hydrodynamic	**Values**
$X_{u\|u\|}$	−48
$Y_{v\|v\|}$	−48
$Z_{w\|w\|}$	−48
$K_{p\|p\|}$	−80
$M_{q\|q\|}$	−80
$N_{r\|r\|}$	−80
$X_{\dot{u}}$	−62.5
$Y_{\dot{v}}$	−62.5
$Z_{\dot{w}}$	−62.5
K_p	−30

used with $s = \sin(\pi/4)$, $l_1 = 0.381$ m, and $l_2 = 0.508$ m, where s, l_1, and l_2 mean nonzero constant factors depending on the thruster allocation.[27–31] The (20) is obtained from (19).[27–31]

$$\mathrm{B}_v = \begin{bmatrix} s & -s & -s & s & 0 & 0 & 0 & 0 \\ s & -s & -s & -s & 0 & 0 & 0 & 0 \\ 0 & 0 & 0 & 0 & -1 & -1 & -1 & -1 \\ 0 & 0 & 0 & 0 & l_1 s & l_1 s & -l_1 s & -l_1 s \\ 0 & 0 & 0 & 0 & l_1 s & -l_1 s & -l_1 s & l_1 s \\ l_2 & -l_2 & l_2 & -l_2 & 0 & 0 & 0 & 0 \end{bmatrix}. \tag{20}$$

The UTS controller (shown in Fig. 3) is composed of three blocks: G/U, ROV, and HEF. The vector position of the human wrist $\mathbf{p}$ is scaled to the URV vehicle domain position $\mathbf{p}_v$, through a simple proportional factor in the G/U block. The $\mathbf{p}_v$ is assumed as the desired trajectory provided as input to the ROV block which generates the actual/real trajectory $\mathbf{p}_r$ (different from $\mathbf{p}_v$ due to the ROV controller error). The difference between the ideal ($\mathbf{p}_v$) and real ($\mathbf{p}_r$) trajectory generates the disturb force $\mathbf{F}_D$.

For the ROV block, six different controllers have been implemented and developed according to state-of-art examples:[27–31] ROV_1;[40] ROV_2;[41] ROV_3;[42] ROV_4;[43] ROV_5;[44] ROV_6.[45]

As regard the HEF (Haptic Error Feedback control system) block, two strategies have been implemented (Fig. 8). The two haptic control systems (H_1 and H_2) are obtained evaluating a force disturb proportional to:

https://doi.org/10.1017/S0263574720000624 Published online by Cambridge University Press

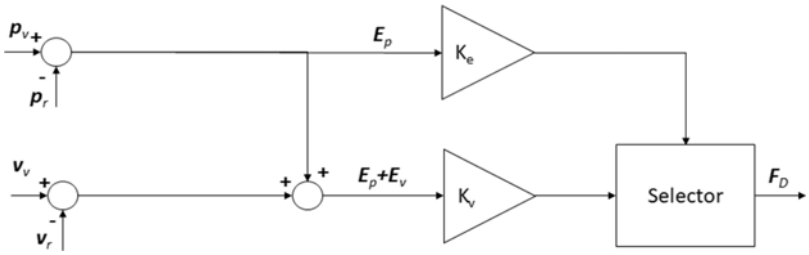


Fig. 8. HEF (haptic error feedback control system) block.

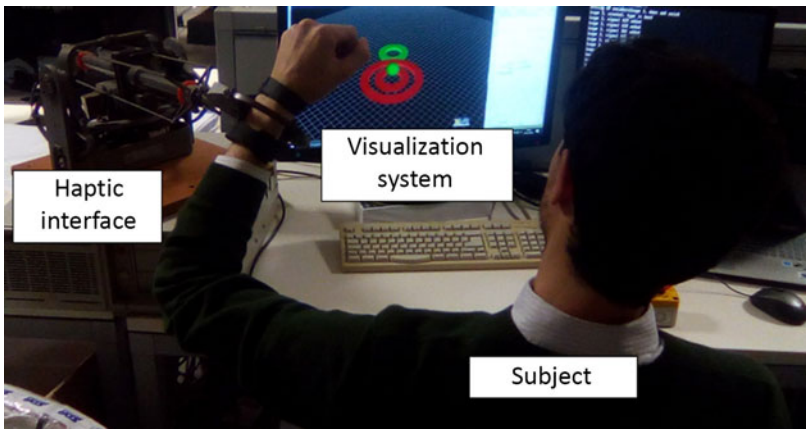


Fig. 9. Real scenario with subject, haptic interface, and visualization system.

- the position errors among the ideal and real ROV trajectory (haptic control 1 (H_1));
- the combination between position and velocity errors among the ideal and real ROV trajectory (haptic control 2 (H_2)).

The two haptic controllers are combined with the six ROV controllers to implement a total of 12 different combinations.

4. Experimentation, Results, and Discussion

4.1. Performed tests

The testing scenario, including the human subject, the visualization system, and the haptic interface, is shown in Fig. 9, while Fig. 10 shows some details of the visualization system. Specifically, the green sphere represents the URV and the three rings (one green and two red) are some references features employed to define two task sequences T1 and T2.

In our experimentations, we tested the two control systems of the haptic interface (H_1, H_2) and the six control systems of the ROV (ROV_1, ROV_2, ROV_3, ROV_4, ROV_5, ROV_6) comparing the performances of the system used by seven subject candidates (named in following: A, B, C, D, E, F, G). A total of 12 experiments have been completed for each subject.

Before starting, each subject tried (for 10 min) to use the complete system with different implemented controls and performing the complete trajectory.

The starting position is shown in Fig. 10 with the URV (green sphere) inside the green ring. From the starting position, the first trajectory to be performed is the T1 which connects the center of the green ring to the center of the red ring. This trajectory must be performed from the starting to the end point and return for a total of eight times. The second trajectory to be performed is T2, and from the starting point, the external red ring must be performed in a clockwise sense before returning in the starting point. The trajectory T2 must be performed for two times.

https://doi.org/10.1017/S0263574720000624 Published online by Cambridge University Press

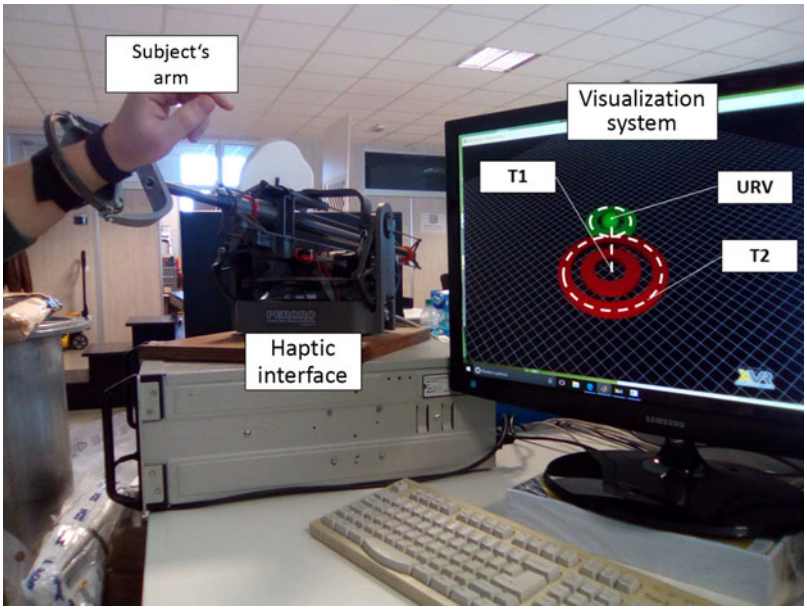


Fig. 10. Visualization system: Trajectories T1 and T2 and URV.

The tests have been performed for all the iterations according to the following sequence:

1. The first subject (or candidate) is positioned and his wrist is connected to the haptic interface.
2. The trajectory to be performed is explained to the first candidate.
3. The system is started and the subject is free to play with the URV performing trajectories with all control systems for 10 min.
4. The 1st haptic control (H_1) is implemented with the first ROV control (ROV_1), and the candidate tries to perform T1 for eight times and T2 for two times.
5. The same trajectories are performed in sequence implementing the first haptic control (H_1) with the 2nd, 3rd, 4th, 5th, 6th ROV control.
6. The same trajectories are performed in sequence implementing the second haptic control (H_2) with the 1st, 2nd, 3rd, 4th, 5th, 6th ROV control.
7. The test is concluded.

4.2. Results and discussion

A comparison between the trajectories T1 and T2, performed by the human wrist of the subject A (scaled in the URV environment), and the URV is presented in Fig. 11, where the coordinates x, y are shown. The trajectory T1 can be identified in the figure by the first four small closed polygons. In particular, each polygon is created by the x and y trajectories of the human wrist and URV starting from the center of the green ring up to the red ring and returning to the start position, as shown in Fig. 10. The trajectory T2 can be noted by the two big polygons after the four small polygons of the trajectory T1. In Fig. 11, the trajectory T1 starts at 25 s and ends at 50 s; the trajectory T2 starts at 50 s and ends at 85 s. The three coordinates x, y, z are shown like in Fig. 1, and the z coordinate shows the deep of the URV in the marine environment.

A detailed analysis of the results allowed us to underline some interesting points. In particular, in this research work, we noted how each subject responds in a different way to the same stimulus. We implemented the same ROV control system and haptic system and noted how each candidate modifies his velocity to perform the trajectory in a different way.

In conclusion, after a first analysis, the haptic controls 1 (H_1) and 2 (H_2) seem to be not completely different, but the haptic controller 1 (H_1) seems to have a smaller error. The ROV controller 1 (ROV_1) seems to have the minimum error between the trajectory of the human wrist and the underwater vehicle.

Figure 12 shows the error comparison between the H_1ROV_1 and H_2ROV_1 controllers for the subject A. It can be seen by the graph how the maximum peak error of the controller H_2ROV_1 is higher

https://doi.org/10.1017/S0263574720000624 Published online by Cambridge University Press

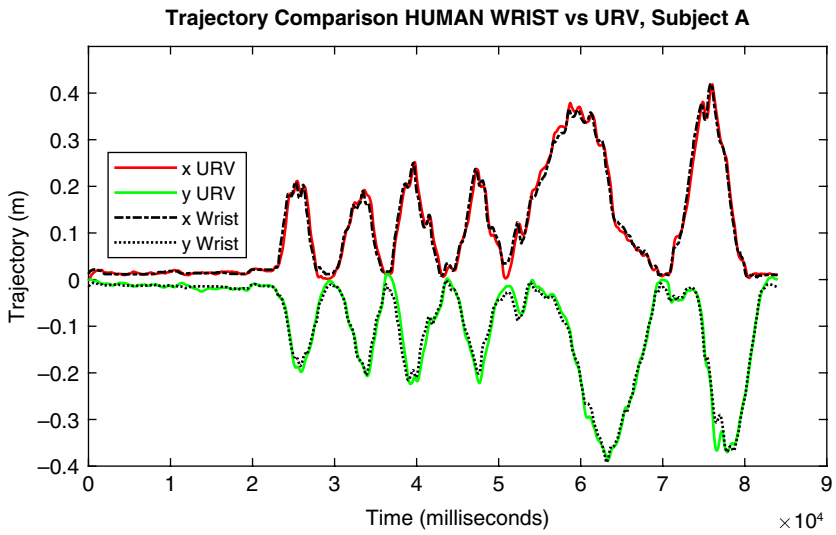


Fig. 11. Trajectory comparison among the x, y coordinates of the human wrist of the subject A (in the URV domain) and the x, y coordinates of the URV.

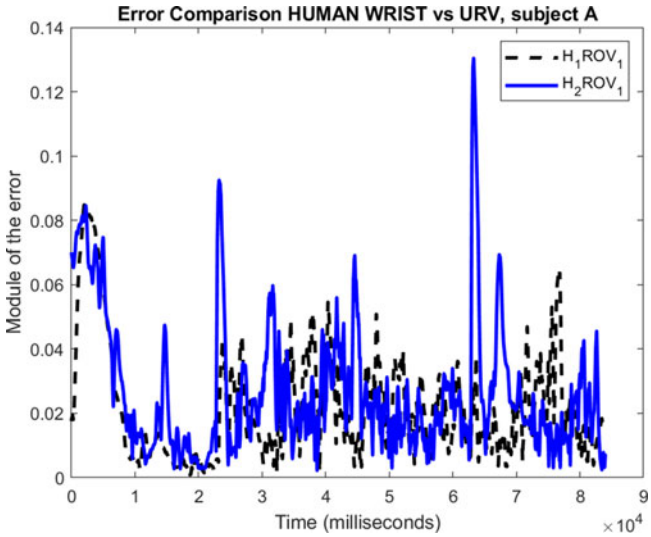


Fig. 12. Error comparison between the H_1 and H_2 controllers for the subject A and the ROV_1 controller.

of the maximum peak error of the H_1ROV_1 controller for the same performed trajectory and the same subject.

In particular, a comparison between the Figs. 11 and 12 allows to underline some preliminary characteristics of the haptic controllers H_2 and H_1. From the Fig. 12, it can be noted how the peaks of the H_2ROV_1 controller are shown at around the same milliseconds of the peaks, as shown in Fig. 11. This underlines that the H_1 controller is not much influenced by the external input like the H_2 controller.

Tables IV and V show the maximum peak (M), the mean (m), and the standard deviation(s) of the module of the error between the trajectory of the human wrist and the URV for each subject and implemented control system. The haptic control H_1 generates the minimum mean of the error between the position of the wrist of the subject (in the URV domain) and the URV position with respect to the haptic control H_2. If the haptic control H_1 is used (see Table IV), the ROV controller to be preferred for implementation is the H_1ROV_1, which reduces the mean. If the haptic control H_2 is used (see Table V), the ROV controllers to be preferred for implementation are the H_2ROV_1 or H_2ROV_5 or H_2ROV_6.

https://doi.org/10.1017/S0263574720000624 Published online by Cambridge University Press

Table IV. Maximum peak (M), mean (m), and standard deviation (s) of the module of the error, for each subject and ROV control system, using the haptic control H_1. The minimum values of the mean (m) are underlined in bold

	A	**B**	**C**	**D**	**E**	**F**	**G**
$M_{H_1ROV_1}$	0.07	0.09	0.11	0.08	0.06	0.07	0.08
$m_{H_1ROV_1}$	**0.02**	**0.01**	**0.03**	**0.03**	**0.01**	**0.03**	**0.02**
$s_{H_1ROV_1}$	0.01	0.01	0.02	0.01	0.01	0.02	0.01
$M_{H_1ROV_2}$	0.12	0.09	0.11	0.11	0.11	0.09	0.10
$m_{H_1ROV_2}$	0.06	0.05	0.06	0.06	0.06	0.06	0.06
$s_{H_1ROV_2}$	0.02	0.01	0.01	0.01	0.01	0.01	0.01
$M_{H_1ROV_3}$	0.08	0.18	0.07	0.11	0.05	0.08	0.07
$m_{H_1ROV_3}$	**0.02**	0.02	**0.03**	**0.03**	0.02	**0.03**	**0.02**
$s_{H_1ROV_3}$	0.01	0.02	0.01	0.02	0.01	0.02	0.01
$M_{H_1ROV_4}$	0.06	0.22	0.08	0.2	0.06	0.1	0.05
$m_{H_1ROV_4}$	**0.02**	0.03	**0.03**	0.04	0.02	**0.03**	**0.02**
$s_{H_1ROV_4}$	0.01	0.03	0.02	0.03	0.01	0.02	0.01
$M_{H_1ROV_5}$	0.15	0.18	0.07	0.14	0.07	0.2	0.07
$m_{H_1ROV_5}$	0.03	0.02	**0.03**	**0.03**	0.02	**0.03**	**0.02**
$s_{H_1ROV_5}$	0.02	0.02	0.01	0.02	0.01	0.03	0.01
$M_{H_1ROV_6}$	0.08	0.1	0.17	0.11	0.11	0.08	0.06
$m_{H_1ROV_6}$	0.03	0.02	0.04	**0.03**	0.02	**0.03**	**0.02**
$s_{H_1ROV_6}$	0.01	0.01	0.03	0.02	0.01	0.01	0.01

Table V. Maximum peak (M), mean (m), and standard deviation (s) of the module of the error, for each subject and control system, using the haptic control H_2. The minimum values of the mean (m) are underlined in bold

	A	**B**	**C**	**D**	**E**	**F**	**G**
$M_{H_2ROV_1}$	0.13	0.05	0.1	0.09	0.06	0.07	0.09
$m_{H_2ROV_1}$	**0.02**	**0.02**	**0.03**	**0.03**	**0.02**	0.03	0.03
$s_{H_2ROV_1}$	0.02	0.01	0.02	0.02	0.01	0.01	0.01
$M_{H_2ROV_2}$	0.12	0.08	0.10	0.1	0.1	0.09	0.1
$m_{H_2ROV_2}$	0.06	0.05	0.06	0.06	0.06	0.06	0.06
$s_{H_2ROV_2}$	0.02	0.01	0.01	0.01	0.01	0.01	0.01
$M_{H_2ROV_3}$	0.13	0.10	0.08	0.11	0.1	0.07	0.13
$m_{H_2ROV_3}$	**0.02**	0.03	**0.03**	**0.03**	0.03	0.03	**0.02**
$s_{H_2ROV_3}$	0.02	0.02	0.02	0.02	0.02	0.02	0.02
$M_{H_2ROV_4}$	0.11	0.1	0.09	0.24	0.1	0.12	0.05
$m_{H_2ROV_4}$	0.02	0.03	**0.03**	**0.03**	**0.02**	0.03	**0.02**
$s_{H_2ROV_4}$	0.02	0.02	0.02	0.03	0.01	0.02	0.01
$M_{H_2ROV_5}$	0.09	0.08	0.18	0.1	0.16	0.07	0.1
$m_{H_2ROV_5}$	0.03	0.03	**0.03**	**0.03**	**0.02**	**0.02**	**0.02**
$s_{H_2ROV_5}$	0.02	0.01	0.03	0.01	0.02	0.02	0.02
$M_{H_2ROV_6}$	0.1	0.08	0.07	0.07	0.06	0.09	0.06
$m_{H_2ROV_6}$	0.03	**0.02**	**0.03**	**0.03**	**0.02**	0.03	**0.02**
$s_{H_2ROV_6}$	0.01	0.02	0.01	0.01	0.01	0.02	0.01

A detailed analysis of all results underlines a unique behavior of the ROV controller 2 (H_1ROV_2 and H_2ROV_2). In particular, Tables IV and V show how the ROV controller 2 (H_1ROV_2 and H_2ROV_2) has higher maximum peaks and mean error values with respect to the others.

Table VI shows the personal evaluation of the used control system, as perceived by the subject, which performed the test. The table shows each subject (A, B, C, D, E, F, G) and the six ROV controllers included with the haptic controls H_1 (H_1ROV_1, H_1ROV_2, H_1ROV_3, H_1ROV_4, H_1ROV_5, H_1ROV_6) and H_2 (H_2ROV_1, H_2ROV_2, H_2ROV_3, H_2ROV_4, H_2ROV_5, H_2ROV_6). Table VI shows in bold the evaluation of the subject for a specific implemented controller as in following: **b**=very bad; **g**=good. Letter n indicates that the subject has not particular notes to underline for the used controller. A comparison among the three Tables IV, V, and VI underlines that the subject does not perceive the variation of the error.

https://doi.org/10.1017/S0263574720000624 Published online by Cambridge University Press

Table VI. Human controller evaluation

	A	**B**	**C**	**D**	**E**	**F**	**G**
H_1ROV_1	n	n	n	n	n	n	n
H_1ROV_2	n	n	n	n	n	n	n
H_1ROV_3	n	n	n	n	n	**g**	n
H_1ROV_4	n	n	n	n	**b**	**g**	n
H_1ROV_5	n	**b**	n	n	n	n	n
H_1ROV_6	n	n	n	**b**	**g**	n	n
H_2ROV_1	n	n	n	n	n	n	n
H_2ROV_2	n	n	n	n	n	**b**	n
H_2ROV_3	n	n	n	n	**b**	n	**b**
H_2ROV_4	n	n	n	n	n	n	n
H_2ROV_5	**b**	n	n	**b**	n	n	n
H_2ROV_6	n	n	n	n	n	n	n

5. Conclusion

In this work, a haptic interface is used by 7 candidates in order to drive a virtual model of a real underwater vehicle and implementing 12 different controllers. A cross comparison among the implemented controllers and the candidates permitted to understand what is the most comfortable controller to drive the model of the real underwater vehicle reducing errors between the trajectory imposed by the human and performed by the underwater vehicle (both in the same scale domain). A perfect control system (in our case) is the one which allows to reproduce a motion of the underwater vehicle in line with the motion of the human's wrist (both in the same scale domain). In this work, the most comfortable controller is the one with minimum error trajectory and a minimum of interaction as underlined by the candidate. This is obtained in particular using a haptic control that provides a feedback that is proportional to the error (i.e., difference between the actual position and the commanded position of the haptic interface) which generates a minimum error between the writs candidate position (in the URV domain) and URV position. Such haptic controller delivers the best user's experience in combination with specific ROV controllers, that is, the trajectory controllers based on earth-fixed-frame-based, model-based controller (ROV_1).[40]

This work draws a first step for understanding a suitable control architecture a haptic-based human–machine interface for underwater robot teleoperation. Future works will be oriented to implement tests for the haptic control systems on a real prototype of underwater vehicle.

Acknowledgments

This research was conducted at the PERCRO (PERCeptual RObotics) laboratory, at Scuola Superiore Sant'Anna, and it is completely supported by the Italian Ministry of Education University and Research, through the SUONO (Safe Underwater Operations iN Oceans) project. Bando MIUR Dectreto direttoriale prot. $N.391/RIC$ del 5/7/12. Smart Cities and Communities.

References

1. S. Sivev, J. Coleman, E. Omerdi, G. Dooly, D. Toal, "Underwater manipulators: A review," *Ocean Eng.*, **163**, 431–450 (2018), ISSN 0029-8018, https://doi.org/10.1016/j.oceaneng.2018.06.018.
2. G. Casalino, et al. "Underwater intervention robotics: An outline of the Italian National Project MARIS." *Marine Technol. Soc. J.* **50**(4), 98–107 (2016).
3. WIMUST European Project, 12 February 2016, http://cordis.europa.eu/project/rcn/194287_en.html
4. S. C. Martin and L. L. Whitcomb, "Fully actuated model-based control with six-degree-of-freedom coupled dynamical plant models for underwater vehicles: Theory and experimental evaluation," *Int. J. Robot. Res.* **35**(10), 1164–1184 (2016). doi: 10.1177/0278364915620032.
5. 12 February 2016 http://ec.europa.eu/maritimeaffairs/policy/blue_growth/index_en.htm
6. V. Iastrebov, G. Seet, T. Asokan, Y. P. Chiu, M. W. S. Lau, "Vision ehancement using stereoscopic telepresence for remotely operated underwater robotic vehicles," *J. Intell. Robot. Syst.* **52**, 139–154 (2008). doi: 10.1007/s10846-008-9203-z.
7. G. G. Muscolo and G. Cannata, "A Novel Tactile Sensor for Underwater Applications: Limits and Perspectives," **In:** *OCEANS 2015*, Genova, 18-21 May (2015), pp. 1–7 doi: 10.1109/OCEANS-Genova.2015.7271717.

https://doi.org/10.1017/S0263574720000624 Published online by Cambridge University Press

8. G. G. Muscolo, G. Moretti and G. Cannata, "SUAS: A novel soft underwater artificial skin with capacitive transducers and hyperelastic membrane," *Robotica* **37**(4), 756–777 (2019). doi: 10.1017/S0263574718001315.
9. A. Aggarwal, P. Kampmann, J. Lemburg and F. Kirchner, "Haptic object recognition in underwater and deep-sea environments," *J. Field Robot*, 1–19 (2015), doi: 10.10027rob.21538.
10. P. Xu, et al., "Design of Control System and Human-Robot-Interaction System of Teleoperation Underwater Robot," **In:** *Intelligent Robotics and Applications* (Springer International Publishing, 2019) pp. , 649–660.
11. J. Zhang, W. Liu, L. Gao, L. Li and Z. Li, "The master adaptive impedance control and slave adaptive neural network control in underwater manipulator uncertainty teleoperation," *Ocean Eng.* **165**, 465–479 (2018), ISSN 0029-8018, https://doi.org/10.1016/j.oceaneng.2018.07.055.
12. R. J. Kuiper, J. C. L. Frumau, F. C. T. van der Helm and D. A. Abbink, "Haptic Support for Bi-Manual Control of a Suspended Grab for Deep-Sea Excavation," **In:** *IEEE International Conference on Systems, Man, and Cybernetics* (2013).
13. A. D. Bowen, D. R. Yoerger, C. Taylor, R. McCabe, J. Howland, D. Gomez-Ibanez, J. C. Kinsey, M. Heintz, G. McDonald, D. B. Peters, B. Fletcher, C. Young, J. Buescher, L. L. Whitcomb, S. C. Martin, S. E. Webster and M. V. Jakuba, "The Nereus Hybrid Underwater Robotic Vehicle for Global Ocean Science Operations to 11,000m Depth," **In:** *OCEANS 2008*, 15–18 September (2008) pp. 1–10. doi: 10.1109/OCEANS.2008.5151993.
14. X. Liang, Y. Li, Z. Peng and J. Zhang, "Nonlinear Dynamics Modeling and Performance Prediction for Underactuated AUV with Fins," **In:** *Nonlinear Dynamics* (Springer Netherlands, 2015).
15. T. W. McLain and S. M. Rock, "Development and experimental validation of an underwater manipulator hydrodynamic model," *Int. J. Robot. Res.* **17**, 748–759, 204 (1988).
16. J. Gancet, et al., "DexROV: Enabling Effective Dexterous ROV Operations in Presence of Communication Latency," **In:** *OCEANS 2015*, 18–21 May, Genova, Italy (2015).
17. R. Bogue, "Underwater robots: A review of technologies and applications," *Ind. Robot Int. J.* **42** (3), 186–191 (2015).
18. R. B. Ambar and S. Sagara, "Development of a master controller for a 3-link dual-arm underwater robot," *Artif. Life Robot.* **20**, 327–335 (2015). doi: 10.1007/s10015-015-0234-9.
19. N. Jamali, P. Kormushev, A. C. Vinas, M. Carreras and D. G. Caldwell, "Underwater Robot-Object Contact Perception Using Machine Learning on Force/Torque Sensor Feedback," **In:** *IEEE International Conference on Robotics and Automation (ICRA)*. Washington State Convention Center. Seattle, Washington, May 26–30 (2015).
20. F. Rydén, A. Stewart and H. J. Chizeck, "Advanced Telerobotic Underwater Manipulation Using Virtual Fixtures and Haptic Rendering," **In:** *OCEANS MTS 2013* (2013).
21. J. J. E. Slotine and W. Li, *Applied Nonlinear Control* (Prentice Hall, New York, 1991).
22. C. S. Ha, S. Park, J. Her, I. Jang, Y. Lee, G. R. Cho, H. I. Son and D. Lee, "Whole-Body Multi-Modal Semi-Autonomous Teleoperation of Mobile Manipulator Systems," **In:** *IEEE International Conference on Robotics and Automation (ICRA)*. Washington State Convention Center. Seattle, Washington, May 26–30 (2015).
23. P. Di Lillo, D. Di Vito, E. Simetti, G. Casalino and G. Antonelli, "Satellite-Based Tele-Operation of an Underwater Vehicle-Manipulator System. Preliminary Experimental Results," **In:** *2018 IEEE International Conference on Robotics and Automation (ICRA)*, Brisbane, QLD, (2018) pp. 7504–7509. doi: 10.1109/ICRA.2018.8462976
24. N. Diolaiti and C. Melchiorri, "Haptic tele-operation of a mobile robot," *IFAC Proc. Vol.* **36**(17), 521–526 (2003).
25. K. D. Le, H. D. Nguyen, D. Ranthumugala and A. Forrets, "Haptic Driving System for Surge Motion Control of Underwater Remotely Operated Vehicles," *Proceedings of 2014 International Conference on Modelling, Identification and Control*, Melbourne, Australia, December 3–5 (2014).
26. G. P. Rosati Papini, M. Fontana and M. Bergamasco, "Desktop haptic interface for simulation of hand-tremor,"*IEEE Trans. Haptics* **9**(1) (2016).
27. G. Antonelli, *Underwater Robots. Motion and Force Control of Vehicle-Manipulator Systems*. Springer Tracts in Advanced Robotics (Springer-Verlag, Heidelberg, Germany, 2003).
28. G. Antonelli, S. Chiaverini, N. Sarkar and M. West, "Adaptive control of an autonomous underwater vehicle: Experimental results on ODIN," *IEEE Trans. Cont. Syst. Technol.* **9**(5) (2001).
29. S. K. Choi, G. Y. Takashige and J. Yuh, "Experimental Study on an Underwater Robotic Vehicle: ODIN," *Proceedings of the 1994 Symposium on Autonomous Underwater Vehicle Technology, AUV 1994*. 19–20 July (1994) pp. 79–84. doi: 10.1109/AUV.1994.518610.
30. H. T. Choi, A. Hanai, S. K. Choi and J. Yuh, "Development of an underwater robot, ODIN-III," *Proceedings of the 2003 IEEE/RSJ International Conference on Intelligent Robots and Systems (IROS 2003)*, vol. 1, 27–31 October (2003) pp. 836–841. doi: 10.1109/IROS.2003.1250733
31. K. D. Do, et al., "A global output-feedback controller for stabilization and tracking of underactuated ODIN: A spherical underwater vehicle," *Automatica* **40**, 117–124 (2004).
32. T. I. Fossen, *Guidance and Control of Ocean Vehicles* (John Wiley and Sons, Chichester, UK, 1994).
33. T. I. Fossen, *Marine Control Systems: Guidance, Navigation and Control of Ships, Rigs and Underwater Vehicles* (Marine Cybernetics AS, Trondheim, Norway, 2002).

https://doi.org/10.1017/S0263574720000624 Published online by Cambridge University Press

34. J. Yuh, "Development in Underwater Robotics," **In:** *IEEE International Conference on Robotics and Automation*, Nagoya, Japan (1995) pp. 1862–1867.
35. J. Yuh, "Exploring the Mysterious Underwater World with Robots," **In:** *6th IFAC Conference on Manoeuvring and Control of Marine Craft*, Girona, Spain (2003).
36. J. Yuh and M. West (2001). "Underwater robotics," *J. Adv. Robot.* **15**, 609–639.
37. T. Ura, "Steps to Intelligent AUVs," **In:** *6th IFAC Conference on Manoeuvring and Control of Marine Craft*, Girona, Spain (2003).
38. SNAME. The Society of Naval Architects and Marine Engineers, "Nomenclature for Treating the Motion of a Submerged Body Through a Fluid," **In:** *Technical and Research Bulletin* (1950) pp. 1–5.
39. K. N. Leabourne, S. M. Rock and M. J. Lee, "Model Development of an Underwater Manipulator for Coordinated Arm-Vehicle Control," **In:** *MTS/IEEE Techno-Ocean 1998*, Nice, France (1998) pp. 941–994.
40. O. Fjellstad and T. I. Fossen, "Position and attitude tracking of AUVs: A quaternion feedback approach," *IEEE J. Oceanic Eng.* **19**, 512–518 (1994).
41. J. Yuh, J. Nie and C. S. G. Lee, "Experimental Study on Adaptive Control of Underwater Robots," **In:** *IEEE International Conference on Robotics and Automation*, Detroit, Michigan (1999) pp. 393–398
42. O. Fjellstad and T. I. Fossen Singularity-Free Tracking of Unmanned Underwater Vehicles in 6DOF. In: *1994 IEEE Conference on Decision and Control*, Lake Buena Vista, Florida (1994) pp. 1128–1133
43. T. I. Fossen and J. Balchen, "The NEROV Autonomous Underwater Vehicle," **In:** *MTS/IEEE Techno-Ocean 1991 Conference*, Honolulu, Hawaii (1991).
44. G. Antonelli, et al., "A Novel Adaptive Control Law for Autonomous Underwater Vehicles," **In:** *IEEE International Conference on Robotics and Automation, ICRA 2001*, vol. 1 (2001) pp. 447–452.
45. Y. C. Sun and C. C. Cheah, "Adaptive Set point Control for Autonomous Underwater Vehicles," **In:** *2003 IEEE Conference on Decision and Control*, Maui, Hawaii (2003) pp. 1262–1267.

https://doi.org/10.1017/S0263574720000624 Published online by Cambridge University Press